land

Potential of Multitemporal Lidar for the Detection of Subtle Archaeological Features under Perennial Dense Forest

Iban Berganzo-Besga [1], Hector A. Orengo [1,2,*], Joan Canela [3] and Maria Carme Belarte [2,3]

1 Landscape Archaeology Research Group (GIAP), Catalan Institute of Classical Archaeology (ICAC), Pl. Rovellat s/n, 43003 Tarragona, Spain
2 Catalan Institution for Research and Advanced Studies (ICREA), Passeig Lluís Companys 23, 08010 Barcelona, Spain
3 Catalan Institute of Classical Archaeology (ICAC), Pl. Rovellat s/n, 43003 Tarragona, Spain
* Correspondence: horengo@icac.cat

Abstract: This paper presents a method for the merging of lidar-derived point clouds of the same area taken at different moments, even when these are not co-registered. The workflow also incorporates the filtering of vegetation allowing the classification of unclassified point clouds using the ground points of reliable coverages. The objective is to produce a digital terrain model by joining all ground points to generate a higher resolution model than would have been possible using a single coverage. The workflow is supplemented by a multi-scale relief visualisation tool that allows for better detection of archaeological micro-reliefs of variable size even in areas of complex topography. The workflow is tested in six Iberian Iron Age sites, all of them located in mountain areas with dense Mediterranean perennial forests and shrub vegetation.

Keywords: remote sensing; lidar; archaeology; iron age; Iberian Peninsula; urbanism; Google Earth Engine

1. Introduction

Lidar-derived digital terrain models (DTMs) have recently become an essential tool in landscape archaeology [1–4]. Besides the important increase in resolution with respect to available global digital surface models (DSMs) such as SRTM, ASTER GDEM, and ALOS, lidar allows the filtering of vegetation cover, buildings, and other human-made structures to produce high-resolution bare-soil DTMs in which archaeological remains can be detected. Raw lidar-derived DTMs only allow the detection of the most evident features and they require the use of DTM visualisation methods to detect subtler topographic changes indicative of the presence of archaeological remains. The combination of lidar-based DTMs and visualisation methods has produced important discoveries in both highly investigated archaeological landscapes and areas that, due to their dense vegetation cover, had not been previously surveyed [5].

However, most lidar applications have been developed in areas with relatively sparse vegetation cover or in deciduous forest areas after leaves have been shed for the season. The use of lidar-derived DTMs for the detection of archaeological structures in areas covered by dense shrubs and perennial forests typical of the Mediterranean has been rather scarce and rarely produces results of equivalent quality as studies that illustrate the potential of the technique [6]. Moreover, many Mediterranean forested areas correspond to mountain environments, which tend to hide micro-reliefs when using standard relief visualisation techniques as these do not respond well to abrupt topographic changes present in mountain areas.

During recent years multitemporal remote sensing data has started to be employed in landscape archaeology to analyse landscape patterns and visualise subtle landscape features [7,8], to detect change affecting archaeological sites [9,10], and to increase the

efficiency of automated site detection methods [11,12]. However, these applications are limited to pixel-based data (mostly multispectral imagery and synthetic aperture radar) and despite the increasing availability of datasets, the combination of lidar coverages acquired during different time periods has rarely been applied for archaeological research.

This paper aims to show how the combined use of multitemporal lidar datasets and multiscale approaches to micro-relief visualisation [13,14] can improve the visualisation of subtle archaeological remains present as micro-reliefs in the ground surface even in complex environments such as forested mountain Mediterranean areas.

2. Case Studies

In order to test our approach, we produced a series of DTMs using multitemporal lidar data from a series of Iberian Iron Age settlements (Figure 1) from which traces of architectural remains have been detected on site but not thoroughly mapped. They all are located in low mountain forested areas. The sites under investigation are described in detail in previous work [15], these correspond to the settlements of:

- Burriac (Cabrera de Mar, Maresme, Barcelona) (41°32′08″ N, 02°23′11″ E) [16]. This large site of around 10 ha corresponds to a first-order settlement, which can probably be identified as ancient Ilturo;
- Castell Barri (Calonge, Baix Empordà, Girona) (41°51′19″ N, 03°02′48″ E). Surface ceramic fragments have been recovered from this second-order town, which provided an approximate dating of 4th–3rd century BC [17];
- Puig d'en Rovira (La Creueta de Quart, Girona) (41°57′48″ N, 02°50′11″ E). This small settlement was occupied from the late 4th to the 2nd century BC [18] with a Roman phase of use during the 1st and 2nd centuries AD;
- Puig Castell (Cànoves i Samalús, Vallès Oriental, Barcelona) (41°41′52″ N, 02°19′30″ E). This is another large (4 ha) first-order settlement that was occupied from the 6th century to the Roman period and probably corresponds to the ancient city of Lauro [19,20];
- Sant Miquel (Vallromanes/Montornès, Vallès Oriental, Barcelona) (41°31′44″ N, 02°16′26″ E). This middle-sized town (1.5–2.5 ha) was occupied from the second half of the 5th to the end of the 2nd century BC [21];
- Torre Roja (Caldes de Montbui, Vallès Oriental, Barcelona) (41°38′00″ N, 02°08′35″ E). This site was occupied from the late 6th century to the Middle Ages. Recent excavations have revealed an Iberian habitation area occupied from the 5/4th to the 1st centuries BC [22].
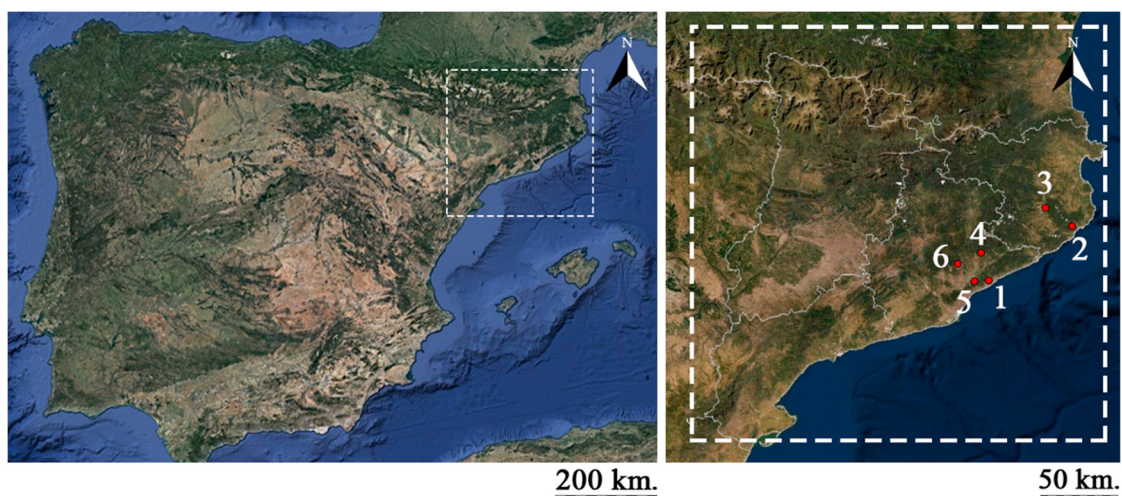
Figure 1. The location of Burriac (1), Castell Barri (2), Puig d'en Rovira (3), Puig Castell (4), Sant Miquel (5), and Torre Roja (6), the settlements under study, in the NE of the Iberian Peninsula (within the white line frame).

The sites that were analysed correspond to birthplaces of the Iberian culture, that spread throughout the Mediterranean area of the Iberian Peninsula. The formation period of this culture corresponds to the Late Bronze Age and Early Iron Age, where a transformation process (increase in population, economic growth, trade with Greeks and Phoenician-Punics, and the introduction of iron) led to the formation of hierarchical societies, the institutionalization of hereditary inequality, and the emergence of political entities that can be considered as early states [23]. Throughout the Early Iberian period, there was a hierarchization of the settlement system, which was organized into nuclei of different sizes and functions, a system that would be clearly consolidated in the Middle Iberian Period (400–200 BC). The first stage of the Roman conquest was characterized by the abandonment and destruction of numerous Iberian settlements as a consequence of the Second Punic War (218–201 BC) military operations and the repression of uprisings by M. Porcius Cato [23,24].

Iberian settlements in the study area are usually classified into four categories, from dispersed rural settlements to urban sites defended by complex fortifications (5 to 10 ha); intermediate categories of sites correspond to villages and fortified sites under 1 ha [25,26]. Common features of Iberian settlements include the preference for settling on low hills with good natural protection, the presence of defensive walls, and an urban plan with houses distributed in rows sharing walls. The main characteristics of the first and second order of settlements, both of which possess urban characteristics, are high density of occupation, urban planning, public buildings, complex dwellings, artisan activities, storage capacity, high-quality imported goods, and evidence of administration. While some towns had some administrative and political control, other settlements had more economic or residential usage.

These settlements all share a common ecosystem and complex topography. The climate of the Catalan area under study, denoted as Csa according to the Köppen classification, is characterized by a temperate climate with dry summers and with an average temperature of above 22 °C during the warmest month. The biogeographic features that characterize the Csa climate are rivers with an irregular regime, vegetation with typical characteristics of semi-arid climates, and reddish-brown soils. The rivers have a lower flow in summer, sometimes drying up, and strong and sudden floods in autumn. The main characteristic of the vegetation is its adaptation to summer heat and dryness through short trunks, thick bark, deep roots, and small strong evergreen leaves. The variable aridity and composition of the soil give rise to four typical formations: herbaceous steppe (more arid, esparto), shrubby steppe (thuyas and dwarf palms), maquis (siliceous soils, undergrowths with heather and isolated trees such as pine trees), and garriga (limestone soils, bare trees where oak is characteristic, and aromatic plants such as thyme). The diverse soils are strongly eroded by heavy rains and deforestation [27].

3. Methods and Sources

A typical lidar system consists of airborne laser scanning (ALS), a GPS-derived aircraft position, an inertial measurement unit (IMU), and the measurement of the deflection angle of the transmitted laser beam. The point clouds generated by this system allow the creation of high-resolution DTMs of the landscape by filtering the points corresponding to vegetation and other elements above the surface of the terrain [28,29]. The remaining points corresponding to the ground surface are usually interpolated to create a continuous raster surface, the DTM. Lidar-derived technologies have been used in multiple disciplines with a geographical basis [30] such as engineering, geomorphology, hydrology, landscape architecture, and archaeology. In archaeology, their most common use, besides GIS-based topographic analysis, has been the detection of archaeological structures visible in the ground surface as topographic imprints. Some of these are very subtle and require specific visualisation techniques for their identification. The use of visualization algorithms can reveal important geomorphological and cultural information [13].

In this study, we employed three different coverages. Initial tests employed the publicly available lidar data at the Cartographic and Geologic Institute of Catalonia (ICGC).

This coverage was obtained from 2008 to 2011. It covered all of the Catalan territories with a minimum density of 0.5 points/m^2. Although in some areas it could reach 4.4 points/m^2 (including all point classes), for the sites under study it ranged from 0.63 points/m^2 for Sant Miquel (acquired in 2008), 0.67 for Burriac (acquired in 2008), 0.74 for Castell Barri (acquired in 2010), 0.91 for Puig Castell (acquired in 2008), and 1.09 for Torre Roja (acquired in 2010) and Puig d'en Rovira (acquired in 2010). The data were calibrated and adjusted with multiple areas of topographic control across the Catalan territory, reaching an average Root Mean Square (RMS) of 6 cm in flat bare soil areas. Lidar point clouds were classified by the ICGC into 14 classes. For the classification of the ground points, besides the automated classification followed for all classes, these were edited manually by an expert. Although of high quality, the testing of this dataset proved the point density to be insufficient in identifying new archaeological structures in the six Iberian settlements. Consequently, a second lidar coverage was carried out specifically for this study. The new dataset was also acquired by the ICGC but with a higher resolution of 5 points/m^2. This dataset was only automatedly classified by the ICGC and incorporated many misclassified points. Several reclassification attempts were made to improve the initial automated classification until a reasonably well-filtered DTM was obtained. Although this DTM provided further insight into the architectural structure of the sites under investigation the improvements were relatively meagre. During the development of the study, the ICGC released a new lidar coverage of Catalonia which was initially acquired between 2016 and 2017, although the areas under interest were all acquired during 2016. This dataset presented similar characteristics to that of the initial publicly available dataset but with a slightly higher point density. The point densities present at the different sites under study were 0.79 for Castell Barri, 0.97 for Puig Castell, 1.05 for Burriac, 1.17 for Sant Miquel, 1.64 for Torre Roja, and 1.73 for Puig d'en Rovira. The DTMs derived from these data did not provide enough topographic information to obtain further insights into the structure of the sites under investigation.

In order to obtain a higher density of points and thereby increase the resolution of the final DTM, we decided to employ all data available within a single workflow (Figure 2). This included all ICGC's coverages (both 2008–2011 and 2016–2017 coverages) and the commissioned lidar data (5 points/m^2). This allowed us to obtain higher-resolution data with an average density of 6–9 points/m^2 (including all point classes). Both public ICGC datasets were already co-registered and well-classified. Although the commissioned coverage presented the highest density of points, these were not co-registered to the publicly available ICGC datasets and their classification was inaccurate. Therefore, it was necessary to co-register this dataset with the others and filter ground points for the development of a DTM integrating all available data.
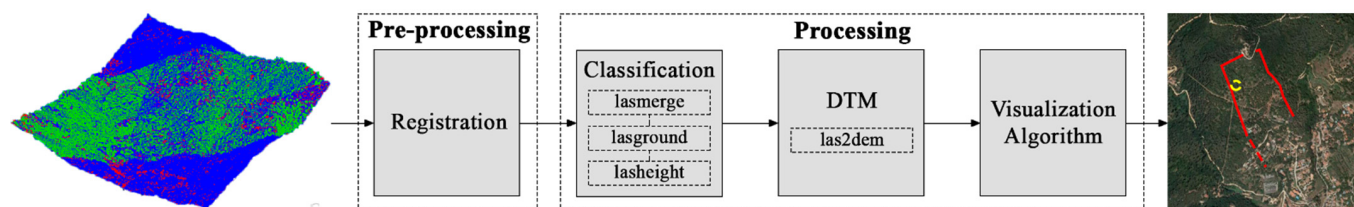

Figure 2. The implemented workflow to detect architectural features from lidar points.

We used the 3D point cloud processing software CloudCompare v2.11.alpha to align the datasets. CloudCompare is a 3D point cloud (and triangular mesh) processing software. It implements the Iterative Closest Point (ICP) algorithm [31] to minimize the difference between two point clouds with an RMS error difference between two iterations lower than the 1.0×10^{-5} threshold. After several co-registration attempts, it became apparent that the best results were obtained when using the combined classified ground points of the public datasets to co-register the ground points of the commissioned lidar data. Although

only the ground points were utilised for the co-registration, the dataset maintained all data which was co-registered during the same process.

The next step consisted of the removal of above-surface features such as buildings and vegetation [1]. As the Csa climate vegetation is arranged in light forest formation with poor ground cover and three layers (trees, shrubs, and herbaceous cover), this step is one of the most crucial to be able to develop a DTM that can reflect small topographic variations. The lidar points were classified using LAStools (Figure 3), a collection of efficient, batch-scriptable, and multicore command line tools.


100 m.
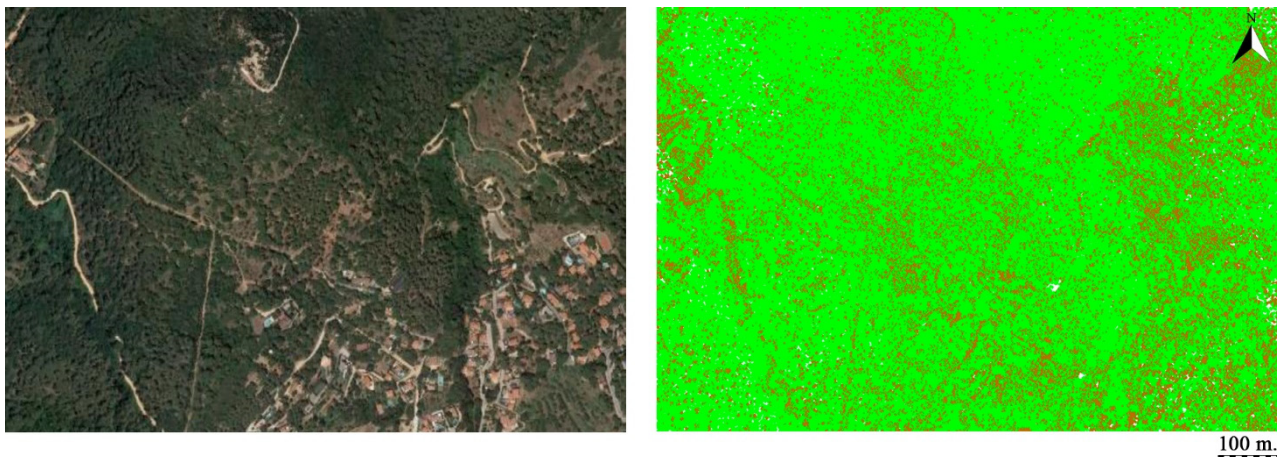
Figure 3. Satellite view (**left**) and classified lidar points (**right**) of the Burriac site.

LAStools also allowed us to merge the co-registered data using its *lasmerge* function and then *lasground* for bare-earth extraction, with the default step parameter of 5.0 which is adequate for forest and mountain environments. For this, the merged point clouds of ground points from both ICGC coverages and the unclassified commissioned coverage were employed. This was the most efficient way to filter low vegetation as the *lasground* was able to employ the bare ground points of the classified coverages to better discriminate points corresponding to vegetation in the unclassified dataset. The *lasground* script classified the lidar points into ground points (*class* = 2) and non-ground points (*class* = 1). The *lasheight* function was used to keep values whose height is between −2 (*drop_below*) and 100 (*drop_above*) meters regarding previously classified terrain. As can be observed in Figure 4, the possible structures of the settlement cannot be seen with the naked eye in the profile view due to their very small overground topography.

The co-registered, merged, and classified data was utilised to generate a DTM using LAStools' *las2dem* function. This tool triangulates lidar points into a triangulated irregular network (TIN), and then rasterises the TIN to create a DTM. The chosen resolution of 0.25 m was chosen given the density of ground points preserved after the classification, which typically amounted to 3–5 points/m^2 in densely forested areas. Thus, choosing this ground resolution for the DTM ensured the highest possible resolution. Using QGIS v3.8 projection tools we assigned ETRS89/UTM zone 31N (EPSG:25831) spatial reference information to each DTM.

Once the filtered high-resolution DTMs for each of the sites under study were obtained, we tested several visualization algorithms to evaluate which one provided a clearer visualization of subtle topographic changes within the DTM. For this, DEM manipulation-based visualization methods (multi-scale relief model (MSRM), simple local relief model (SLRM), and slope gradient), illumination-based ones (principal component analysis of multi-azimuth shaded relief maps, which is not kernel-size dependent), and other kernel-size dependent techniques (Sky-View Factor (SVF) and Opennes) were selected [29,32–34].
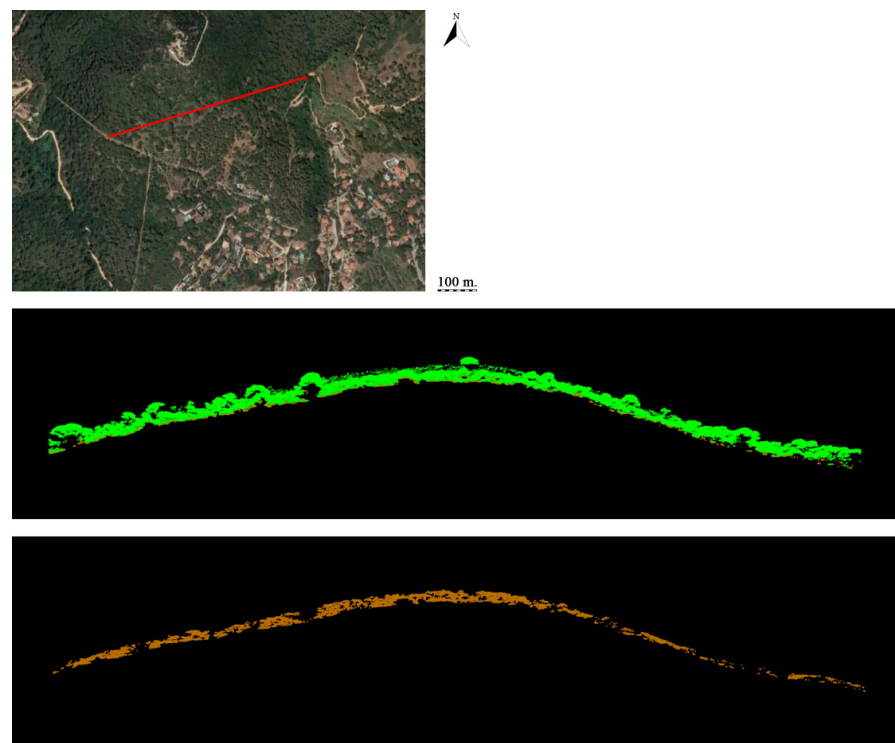
Figure 4. Profile view of the Burriac site (**centre**) and the same profile but only with the ground points (*class* = 2) (**bottom**). The cut (red) is indicated in the satellite view of the site (**top**).

The best results were obtained using the MSRM (*fmn* = 0, *fmx* = 30, *x* = 1). Concerning the rest, the only one that showed results similar to the MSRM was the SLRM (*radius* = 30) (Figure 5). The noticeably better visualisation provided by MSRM method is probably due to its capacity to show microtopographic imprints at variable scales. Recent comparisons between multi-scale topographic visualisation, single-scale, and illumination-based methods [12,14] show that multi-scale visualisation methods also produce better results for the automated detection of structures in lidar data using deep learning detectors. This implies a more coherent visualisation of features at slightly different scales. Google Earth Engine Code Editor, Repository and Cloud Computing Platform [35] was used to obtain the MSRM raster and The Relief Visualization Toolbox (RVT) for the other relief visualisation methods [34].
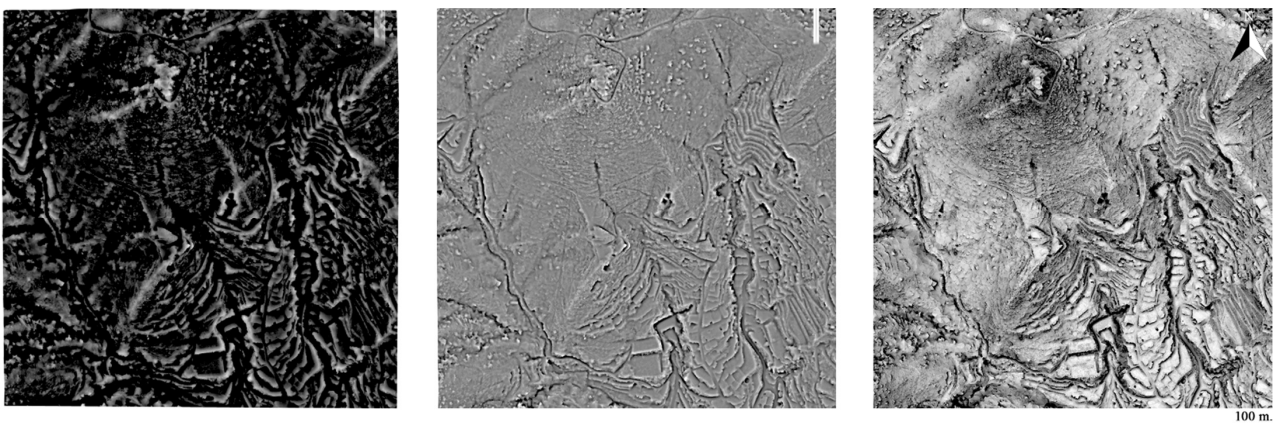
Figure 5. Comparison for the Burriac settlement of the different visualization algorithms, which have been shown to be better for the case study: MSRM, SLRM, and SVF (from left to right).

4. Results

Previous research [15] based on commissioned lidar coverage presents a much lower density of points, inaccurately classified ground points, and unsophisticated visualisation methods. Unsurprisingly, comparison with the newly developed workflow shows notable improvements in the visualisation of the walled structures around five of the six archaeological sites under study (Figure 6). The following paragraphs will briefly describe the results obtained using the workflow described above for each of the six settlements under consideration.
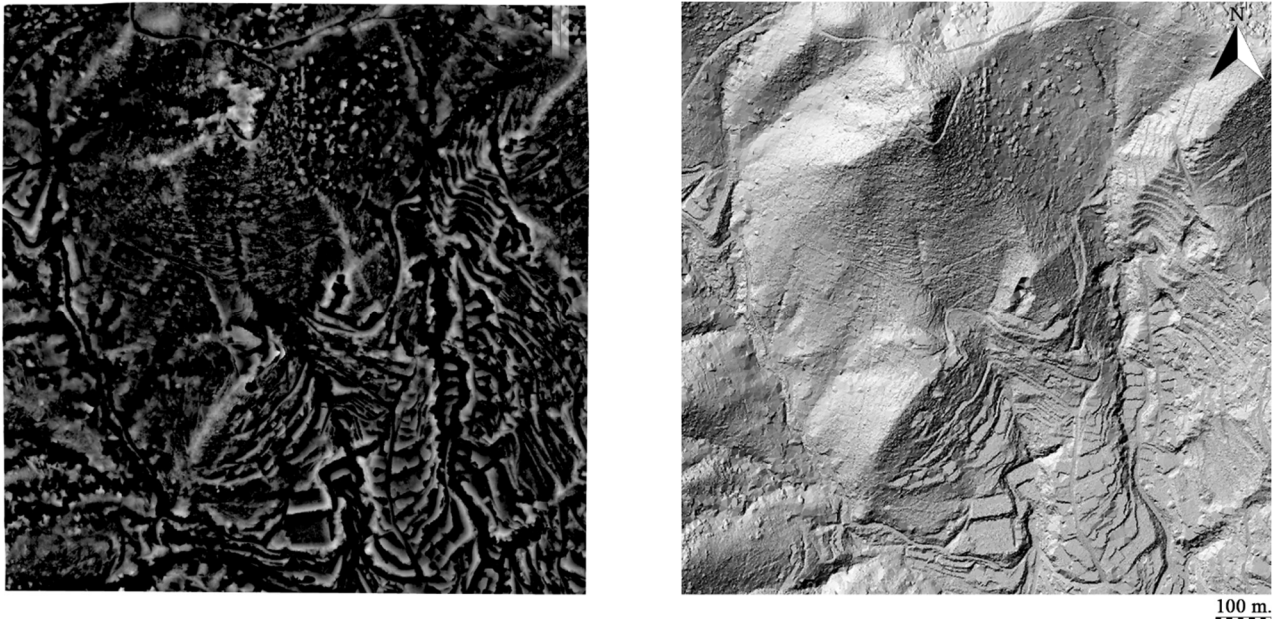
Figure 6. MSRM (**left**) and hillshade (**right**) of the Burriac site.

The site of Puig Castell (Cànoves i Samalús, Vallès Oriental, Barcelona) presents a continuous view of the whole fortified enclosure wall. The settlement extends in a northwest–southeast direction. We did not identify any rooms inside the rampart, but we recognized one more wall in the north–south direction in the southern part of the walled area (Figure 7) which could have formed part of a hallway or walled access to the site.
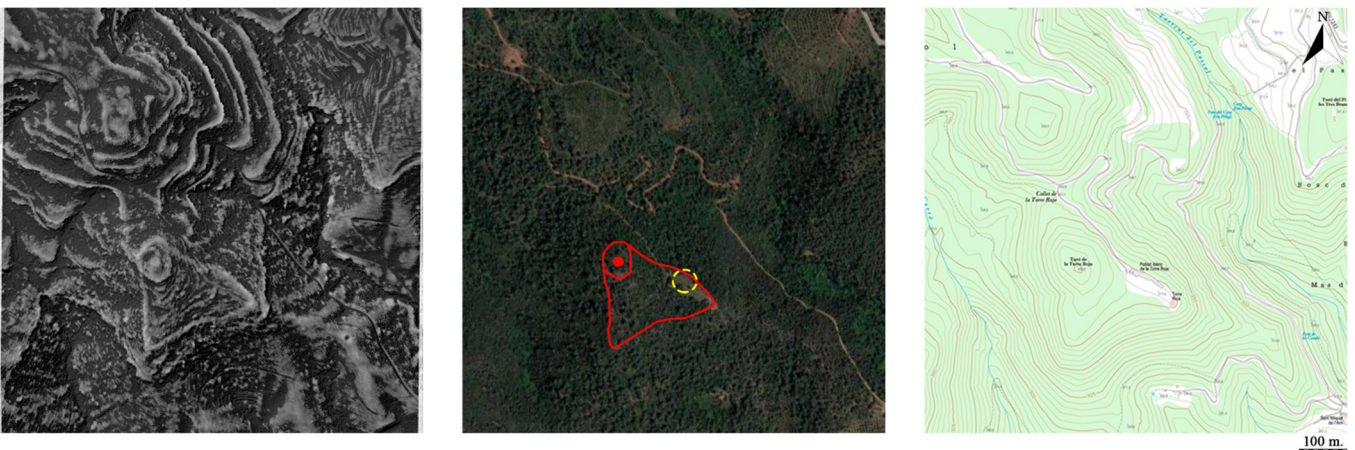

Figure 7. MSRM (**left**), satellite view (**centre**) and topographic map (**right**, forest in green) of the Puig Castell site. In the satellite image the walls (red) and the known location of the settlement (yellow) are indicated.

At Burriac (Cabrera de Mar, Maresme, Barcelona) most of the walled enclosure of the northwest part has been detected. The settlement extends in a northwest–southeast direction (Figure 8).

Figure 8. MSRM (**left**), satellite view (**centre**) and topographic map (**right,** forest in green) of the Burriac site. In the satellite image the walls (red) and the known location of the settlement (yellow) are indicated.

The analysis of Torre Roja (Caldes de Montbui, Vallès Oriental, Barcelona) shows a triangular walled enclosure structure. The settlement extends in a northwest–southeast direction. Moreover, an interior circular structure is observed in the northwest (Figure 9).

Figure 9. MSRM (**left**), satellite view (**centre**) and topographic map (**right**, forest in green) of the Torre Roja site. In the satellite image the walls (red) and the known location of the settlement (yellow) are indicated.

The analysis of Castell Barri (Calonge, Baix Empordà, Girona) shows a large part of the perimeter wall structure. The settlement extends in a northeast–southwest direction. We were able to detect a possible additional wall in the northeast (Figure 10).

In the case of Puig d'en Rovira (La Creueta de Quart, Girona), although the visibility of this settlement is poorer than that of the other sites, almost the entire wall structure can be observed. The settlement extends in a north–south direction. Similar to previous cases, there are no signs of interior rooms (Figure 11).

Finally, analysis of Sant Miquel (Vallromanes/Montornès, Vallès Oriental, Barcelona) resulted in detection of several sections of wall structures. The settlement extends in a northeast–southwest direction. Two parallel walls are clearly observed in a northeast–

southwest direction. In addition, the closing wall of the settlement in the northeast area is observed (Figure 12).

Figure 10. MSRM (**left**), satellite view (**centre**) and topographic map (**right**, forest in green) of the Castell Barri site. In the satellite image the walls (red) and the known location of the settlement (yellow) are indicated.

Figure 11. MSRM (**left**), satellite view (**centre**) and topographic map (**right**, forest in green) of the Puig d'en Rovira site. In the satellite image the walls (red) and the known location of the settlement (yellow) are indicated.

Figure 12. MSRM (**left**), satellite view (**centre**) and topographic map (**right**, forest in green) of the Sant Miquel site. In the satellite image the walls (red) and the known location of the settlement (yellow) are indicated.

5. Discussion

In the presented case-study, a combination of airborne lidar coverages and a multi-scale visualisation algorithm provided useful insights in all the study sites, which were located in a Mediterranean Csa environment. The results show noticeable improvement with respect to the use of a single coverage as shown in a previous study [15]. We sought to improve the visibility of archaeology-related micro-reliefs by increasing the ground point density and quality as well as employing more suitable visualization algorithms. The increase in the density of points using a purposely commissioned lidar coverage and the two public access coverages of the ICGC enabled the detection of most sites' perimeter walls and some inner large structures in the Castell Barri and Torre Roja settlements. Despite this, clear identification of smaller structures, such as the walls of houses, remains a challenge. To achieve this, a much higher point density is necessary, which will, perhaps, be achieved as more sophisticate lidar coverages become available in the future.

In any case, the delimitation of the walls and the potential extension of the archaeological sites provides important new data as:

1. It will allow for the estimation of the potential population and hierarchies between sites;
2. It will allow for the development of conscientious excavation planning, which can now focus on intramural areas and not waste efforts in potentially uninhabited sectors;
3. It will allow for more informed heritage protection measures, which will be able to take into account the site as a whole and not just the small area where remains have been detected.

The workflow presented here provides a way to co-register and filter several point clouds to increase the resolution of a DTM and, by doing so, improve the detection of subtle topographic features even in complex areas where perennial forests and shrubs combine with abrupt slopes. As many countries such as Portugal start to develop large public lidar datasets and others such as Spain, the UK, and the Netherlands have already made available multiple coverages for the same areas, the use of this and similar workflows offer a way to increase the DTM resolution and boost the detection of archaeological micro-reliefs, which are not easily identifiable in single national coverages as these rarely implement the necessary resolution.

This workflow also provides a way to combine and integrate different types of data as point clouds when a single one of those presents reliable ground points. This can be used, for example when well-classified lidar point clouds are available but these do not have enough resolution. In this case, this workflow can be implemented using the lidar ground points to register and classify photogrammetry-derived point clouds obtained, for example, with increasingly accessible UAVs or drones. Another option is the use of DGPS-derived points as the ground points which can be combined with lidar, photogrammetry-derived, or both types of point clouds. By providing a way to integrate and improve point data obtained over several periods, with different means, and at different resolutions and qualities, the proposed workflow provides an efficient way to reuse legacy data, which is widely encouraged within the discipline (e.g., [36,37]).

6. Conclusions

The field of landscape archaeology is rapidly developing toward the use of big structured and unstructured data. New trends such as the development of data fusion methods for multitemporal and multisource data in virtual satellite constellations [10,11] and the creation of virtual data through data augmentation processes hold much potential for the development of more holistic analysis with deeper analytical capabilities. Point cloud-data, in particular, can benefit from new approaches since many of the methods employed in archaeological surveys such as lidar, terrestrial laser scanning and total stations, differential GPS, and photogrammetry generate cloud points. Being able to use a reliable reference dataset to structure all these diverse data through correlation, filtering, and classification methods has the potential to radically improve archaeological surveys and the detection and analysis of microtopographic archaeological features.

In this paper we presented a method for the merging and filtering of point clouds and their analysis using multiscale relief visualisation methods. Hopefully, similar workflows can unleash the emerging potential behind other sources of georeferenced point clouds.

Author Contributions: I.B.-B. and H.A.O. wrote the original paper. I.B.-B. conducted the analysis and produced the images; H.A.O. revised the text, designed the methods, and supervised the research; J.C. collected and curated the commissioned lidar data; M.C.B. contributed to the revision of the text, directed the project, and obtained the funds for the commissioned lidar data. All authors have read and agreed to the published version of the manuscript.

Institutional Review Board Statement: Not applicable.

Informed Consent Statement: Not applicable.

Data Availability Statement: Not applicable.

Conflicts of Interest: The authors declare no conflict of interest.

References

1. Bewley, R.; Crutchley, S.; Shell, C. New light on an ancient landscape: LIDAR survey in the Stonehenge World Heritage Site. *Antiquity* **2005**, *79*, 636–647. [CrossRef]
2. Evans, D.; Pottier, C.; Fletcher, R.; Hensley, S.; Tapley, I.; Milne, A.; Barbetti, M. A comprehensive archaeological map of the world's largest preindustrial settlement complex at Angkor, Cambodia. *Proc. Natl. Acad. Sci. USA* **2007**, *104*, 14277–14282. [CrossRef] [PubMed]
3. Opitz, R.S.; Ryzewski, K.; Cherry, J.F.; Malone, B. Using airborne LiDAR Survey to explore historic-era archaeological landscapes of Montserrat in the eastern Caribbean. *J. Field Archaeol.* **2015**, *40*, 523–541. [CrossRef]
4. Parcero-Oubiña, C. At Last! Remote-Sensing Discovery of Archaeological Features through Aerial Imagery and Lidar in Galician Hillforts. *AARGnews* **2022**, *64*, 22–33.
5. Amable, G.; Devereux, B.; Crow, P.; Cliff, A.D. The potential of airborne LiDAR for detection of archaeological features under woodland canopies. *Antiquity* **2005**, *79*, 648–660.
6. Doneus, M.; Mandlburger, G.; Doneus, N. Archaeological Ground Point Filtering of Airborne Laser Scan Derived Point-Clouds in a Difficult Mediterranean Environment. *JCAA* **2020**, *3*, 92–108. [CrossRef]
7. Orengo, H.A.; Petrie, C.A. Large-scale, multi-temporal remote sensing of palaeo-river networks: A case study from northwest India and its implications for the Indus Civilisation. *Remote Sens.* **2017**, *9*, 735. [CrossRef]
8. Garcia, A.; Orengo, H.A.; Conesa, F.C.; Green, A.S.; Petrie, C.A. Remote Sensing and Historical Morphodynamics of Alluvial Plains. The 1909 Indus Flood and the City of Dera Ghazi Khan (Province of Punjab, Pakistan). *Geosciences* **2019**, *9*, 21. [CrossRef]
9. Rayne, L.; Gatto, M.C.; Abdulaati, L.; Al-Haddad, M.; Sterry, M.; Sheldrick, N.; Mattingly, D. Detecting Change at Archaeological Sites in North Africa Using Open-Source Satellite Imagery. *Remote Sens.* **2020**, *12*, 3694. [CrossRef]
10. Agapiou, A.; Alexakis, D.D.; Hadjimitsis, D.G. Potential of virtual earth observation constellations in archaeological research. *Sensors* **2019**, *19*, 4066. [CrossRef]
11. Orengo, H.A.; Conesa, F.C.; Garcia-Molsosa, A.; Lobo, A.; Green, A.S.; Madella, M.; Petrie, C.A. Automated detection of archaeological mounds using machine learning classification of multi-sensor and multi-temporal satellite data. *Proc. Natl. Acad. Sci. USA* **2020**, *117*, 18240–18250. [CrossRef] [PubMed]
12. Berganzo-Besga, I.; Orengo, H.A.; Lumbreras, F.; Carrero-Pazos, M.; Fonte, J.; Vilas-Estévez, B. Hybrid MSRM-Based Deep Learning and Multitemporal Sentinel 2-Based Machine Learning Algorithm Detects Near 10k Archaeological Tumuli in North-Western Iberia. *Remote Sens.* **2021**, *13*, 4181. [CrossRef]
13. Orengo, H.A.; Petrie, C.A. Multi-scale relief model (MSRM): A new algorithm for the visualization of subtle topographic change of variable size in digital elevation models. *Earth Surf. Process. Landf.* **2018**, *43*, 1361–1369. [CrossRef] [PubMed]
14. Guyot, A.; Lennon, M.; Hubert-Moy, L. Objective comparison of relief visualization techniques with deep CNN for archaeology. *J. Archaeol. Sci. Rep.* **2021**, *38*, 103027. [CrossRef]
15. Belarte, M.C.; Canela, J.; Orengo, H.A.; Berganzo-Besga, I. Using LIDAR to detect architectural features in urban sites in the coast of Northern Iberia (6th–3rd centuries BC). In *Urbanization in Iberia and Mediterranean Gaul in the First Millennium BC*, 1st ed.; Treballs de la Mediterrània Antiga, 7, Belarte, M.C., Noguera, J., Plana-Mallart, R., Sanmartí, J., Eds.; ICAC: Tarragona, Spain, 2020; Volume 1, pp. 137–148.

16. Barberà, J.; Pascual, R. Burriac, un yacimiento protohistórico de la costa catalana (Cabrera de Mar, Barcelona). *Ampurias* **1980**, *41–42*, 203–242.

17. Oliva, M. El poblado ibérico de Castell Barri. *Ampurias* **1947**, *9–10*, 288–293.

18. Riuró, F. El poblado de La Creueta. *Ampurias* **1943**, *5*, 117–131.

19. Estrada, J. *Síntesis Arqueológica de Granollers y sus Alrededores*, 1st ed.; Museo de Granollers: Granollers, Spain, 1955.

20. Garcia Molsosa, A.; Flórez Santasusana, M.; Palet Martínez, J.M. Arqueología del paisaje en el entorno de «Lauro»: Una aproximación microrregional a la construcción del territorio romano en el noreste de la Península Ibérica. *Zephyrus* **2015**, *76*, 99–119.

21. Asensio, D.; Guitart, J. *El Jaciment ibèric de la Muntanya de Sant Miquel. Montornès del Vallès i Vallromanes. Recull de Documentació i assaig d'interpretació*, 1st ed.; Diputació de Barcelona: Barcelona, Spain, 2010.

22. Fortó, A.; Maese, X. La Torre Roja: Un jaciment ibèric i medieval (Caldes de Montbui, Vallès Oriental; Sentmenat, Vallès Occidental). *Trib. D'arqueologia* **2010**, *2009–2010*, 113–152.

23. Sanmartí, J. From the archaic states to romanization: A historical and evolutionary perspective on the Iberians. *Catalan Hist. Rev.* **2009**, *2*, 9–32.

24. (Coord) Fernández, A.; Hernando, A.; Maillo, J.M.; Muñoz, F.J.; Quesada, J.M.; Ripoll, S. *Prehistoria II. Las sociedades metalúrgicas*, 2nd ed.; Editorial Universitaria Ramón Areces: Madrid, Spain, 2015; pp. 665–689.

25. Asensio, D.; Morer, J.; Rigo, A.; Sanmartí, J. Les formes d'organització social i económica a la Cossetània ibèrica: Noves dades sobre l'evolució i tipología dels assentaments entre els segles VII-I a.C. In *Territori Polític i Territori Rural Durant L'edat del Ferro a la Mediterrània Occidental. Actes de la Taula Rodona celebrada a Ullastret*, 1st ed.; Martí, A., Plana, R., Eds.; Museu d'Arqueologia de Catalunya-Ullastret: Girona, Spain, 2001; Volume 1, pp. 253–271.

26. Orengo, H.A.; Ejarque, A.; Albiach, R. Water management and land-use practices from the Iron-Age to the Roman period in Eastern Iberia. *J. Archaeol. Sci.* **2014**, *49*, 265–275. [CrossRef]

27. Aguilera, M.J.; Borderías, M.P.; González, M.P.; Santos, J.M. *Geografía General I (Geografía Física)*, 1st ed.; Editorial Universidad Nacional de Educación a Distancia: Madrid, Spain, 2009; pp. 266–271.

28. Wehr, A.; Lohr, U. Airborne laser scanning—An introduction and overview. *ISPRS J. Photogramm. Remote Sens.* **1999**, *54*, 68–82. [CrossRef]

29. Hesse, R. LiDAR-derived Local Relief Models—A new tool for archaeological prospection. *Archaeol. Prospect.* **2010**, *17*, 67–72. [CrossRef]

30. Gutiérrez-Antuñano, M.A.; Tiana-Alsina, J.; Rocadenbosch, F.; Sospedra, J.; Aghabi, R.; González-Marco, D. A wind-lidar buoy for offshore wind measurements: First commissioning test-phase results. In *IEEE International Geoscience and Remote Sensing Symposium (IGARSS)*, 1st ed.; IEEE: Fort Worth, TX, USA, 2017; pp. 1607–1610.

31. Besl, P.J.; McKay, N.D. A method for registration of 3-D shapes. In *IEEE Transactions on Pattern Analysis and Machine Intelligence*; IEEE Computer Society: Washington, DC, USA, 1992; Volume 14, pp. 239–256. [CrossRef]

32. Zakšek, K.; Oštir, K.; Kokalj, Ž. Sky-View Factor as a Relief Visualization Technique. *Remote Sens.* **2011**, *3*, 398–415. [CrossRef]

33. Doneus, M. Openness as Visualization Technique for Interpretative Mapping of Airborne Lidar Derived Digital Terrain Models. *Remote Sens.* **2013**, *5*, 6427–6442. [CrossRef]

34. Kokalj, Ž.; Hesse, R. *Airborne Laser Scanning Raster Data Visualization: A Guide to Good Practice*, 1st ed.; Založba ZRC: Ljubljana, Slovenia, 2017.

35. Gorelick, N.; Hancher, M.; Dixon, M.; Ilyushchenko, S.; Thau, D.; Moore, R. Google Earth Engine: Planetary-scale geospatial analysis for everyone. *Remote Sens. Environ.* **2017**, *202*, 18–27. [CrossRef]

36. Faniel, I.; Kansa, E.; Whitcher Kansa, S.; Barrera-Gomez, J.; Yakel, E. The challenges of digging data: A study of context in archaeological data reuse. In Proceedings of the 13th ACM/IEEE-CS Joint Conference on Digital Libraries, Indianapolis, IN, USA, 22–26 July 2013; ACM: New York, NY, USA, 2013; pp. 295–304.

37. Opitz, R.; Herrmann, J. Recent Trends and Long-standing Problems in Archaeological Remote Sensing. *J. Comput. Appl. Archaeol.* **2018**, *1*, 19–41. [CrossRef]